In Situ Monitoring of Intracellular Controlled Drug Release from Mesoporous Silica Nanoparticles Coated with pH-Responsive Charge-Reversal Polymer

Peng Zhang, Tong Wu, and Ji-Lie Kong*

Department of Chemistry and Institutes of Biomedical Sciences, Fudan University, Shanghai 200433, China

S *Supporting Information*

ABSTRACT: Therapeutic platforms such as chemotherapy that respond to physical and biological stimuli are highly desirable for effective cancer therapy. In this study, pH-responsive charge-reversal, polymer-coated mesoporous silica nanoparticles [PAH-cit/APTES-MSNs; PAH-cit refers to poly(allylamine)−citraconic anhydride; APTES refers to (3-aminopropyl)triethoxysilane] were synthesized for application as drug-delivery systems for the treatment of malignant cells. Confocal laser scanning microscopy (CLSM) revealed that the PAH-cit/APTES-MSNs nanocomposite effectively delivered and released doxorubicin hydrochloride to the nucleus of HeLa (human cervical carcinoma) cells. Additionally, the real-time dynamic drug-release process was monitored by CLSM. The current pH-controlled-smart-release platform holds promise in drug-delivery and cancer therapy-related applications.

KEYWORDS: *mesoporous silica nanoparticles, drug delivery, pH-controlled release, pH-responsive charge-reversal polymer, doxorubicin hydrochloride*
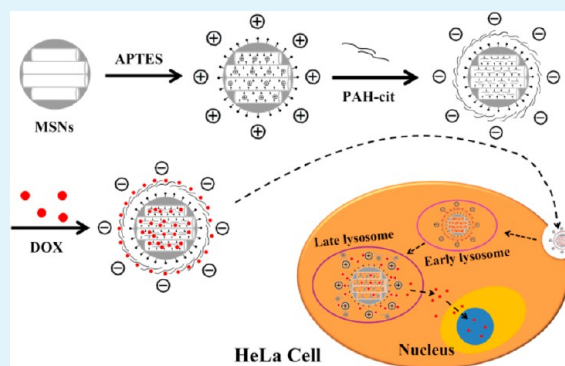
1. INTRODUCTION

Drug delivery systems (DDSs) are known to improve the performance of traditional chemotherapy by reducing side effects on the healthy cells and enhancing targeted drug delivery to the malignant cells through enhanced permeability and retention effects.[1] In the past years, organic materials have been used as drug carriers such as liposomes,[2,3] micelles,[4,5] and dendrimers.[6] However, they suffer from poor stability, which restricts their application owing to biochemical attacks. Recently, mesoporous silica nanoparticles (MSNs) have emerged as promising drug-delivery carriers owing to their unique mesoporous structures, large surface areas, high chemical stabilities, good biocompatibilities, and ease of functionalization.[7−16] A series of MSN-related DDSs have been developed during the past decade, and different stimuli have been employed as triggers for controlled drug release such as enzymes,[17−21] light/irradiation,[22−25] pH,[26−31] and redox reactions.[32−39] Among these stimuli-controlled-release systems, pH-responsive DDSs show great advantages because tumors exhibit lower pH environments compared with normal cells, especially in intracellular endosomes and lysosomes.[40]

Nanoparticles (NPs)[24,27,32,35] or polymers[28,36,37,41−43] are usually employed as cappers to seal the pores of MSNs to prevent premature drug release. Compared with NPs, polymers are a better option because NPs−NPs hybrid systems are more complicated to synthesize than polymer−NPs hybrid systems. Furthermore, the subsequent removal of NPs may induce toxic reactions to human bodies. Yang et al.[42] fabricated pH-sensitive polymer-coated MSNs using in situ polymerization for pH-controlled doxorubicin hydrochloride (DOX) release. Additionally, Hu et al.[43] constructed pH-responsive poly(acrylic acid)-coated MSNs, which were applied to pH-controlled drug delivery. However, both developed DDSs have the following limitation: drug release at the desired pH condition is hindered because the polymer molecules are covalently functionalized on the MSN surface.

Poly(allylamine)−citraconic anhydride (PAH-cit) is a pH-responsive charge-reversal polymer, whereby the charge can be readily converted from negative to positive through side-chain hydrolysis upon exposure to acid solutions (Figure 1a,c). Using this property, Liang et al.[44,45] fabricated gold-nanoparticle-based, pH-controlled nucleic acid delivery/release systems; the results showed that siRNA was effectively delivered and released to cancer cells. Zhou et al.[46] constructed a pH-controlled drug-delivery/release nanocomplex based on PAH-cit and graphene oxide (GO). The GO/PEI/PAH-cit-DOX [PEI refers to poly(ethylenimine)] multilayer was constructed through electrostatic forces. At low pH, the conjugated DOX was released from the nanocomposite because of amide hydrolysis of PAH-cit. In vitro experiments demonstrated that
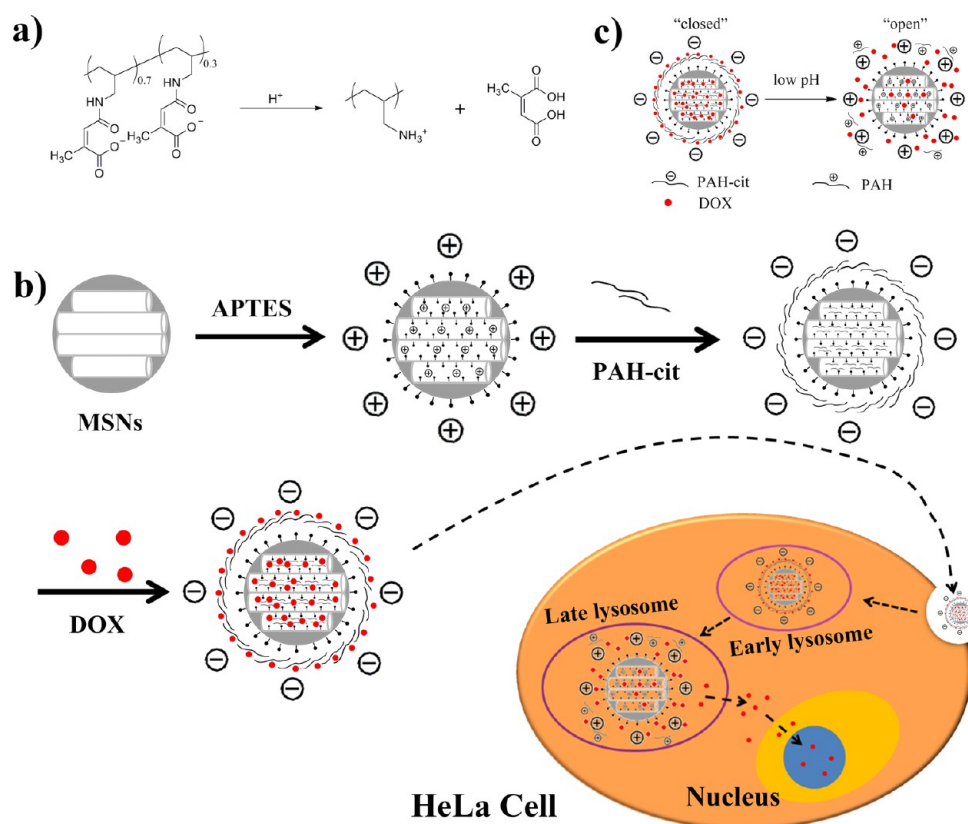
Figure 1. (a) Hydrolysis of PAH-cit in acidic environments yielding cationic PAH. (b) Synthesis of DOX@PAH-cit/APTES-MSNs-based pH-controlled-release system and controlled release of DOX at lysosome (or endosome) inside HeLa cells. (c) Rupture of a DOX@PAH-cit/APTES-MSNs nanocomposite under low-pH conditions.

this nanocarrier could load DOX with high efficiency and that DOX was efficiently released in acidic environments.

In this work, pH-responsive charge-reversal polymer-coated MSNs were prepared as a DDS for controlled drug release. Compared with the complex delivery system developed by Zhou et al.,[46] our developed system is simpler, especially in view of the nanocarrier synthesis and drug loading. DOX was employed as a model anticancer drug to evaluate the loading and controlled-release ability of PAH-cit/APTES-MSNs [APTES refers to (3-aminopropyl)triethoxysilane]. In acidic environments, the loaded DOX was steadily released from the MSNs as a result of strong electrostatic repulsion forces among the positively charged MSNs (APTES-MSNs), PAH, and DOX. The cytotoxic effect of the DOX@PAH-cit/APTES-MSNs nanocomposite on HeLa (human cervical carcinoma) cells was examined by an MTT [3-(4,5-dimethylthiazol-2-yl)-2,5-diphenyltetrazolium bromide] assay that showed effective eradication ability. A real-time monitoring experiment was conducted using confocal laser scanning microscopy (CLSM) to obtain information relating to drug release from the DOX@PAH-cit/APTES-MSNs nanocomposite and subsequent location and activity of the released DOX.

2. EXPERIMENTAL SECTION

2.1. Materials. Tetraethylorthosilicate (TEOS) and APTES were purchased from Sigma-Aldrich (St. Louis, MO). PAH (M_w = 15000) was purchased from Sigma. PAH-cit was synthesized using the reported procedure.[47] Cetyltrimethylammonium bromide (CTAB) was purchased from Alfa Aesar (Tianjin, China). DOX was purchased from Beijing HuaFeng United Technology Co., Ltd. (China). Dulbecco's modified Eagle's medium (DMEM) and fetal calf serum

(FCS) were purchased from GBICO. 2-(4-Amidinophenyl)-6-indolecarbamidine dihydrochloride (DAPI) was purchased from KeyGen Biotech Co., Ltd. (Nanjing, China). All chemicals were of analytical grade and were used without further purification. Deionized water was used in all experiments and analyses.

2.2. Synthesis of MSNs. The synthesis of MSNs was performed using a previously published report.[48] Briefly, CTAB (0.5 g) was dissolved in deionized water (250 mL). A sodium hydroxide aqueous solution (2.00 M, 1.75 mL) was added to the CTAB solution, and the temperature of the mixture was adjusted to 80 °C. Then, TEOS (2.5 mL) was added to the above solution under vigorous stirring. The mixture was allowed to react for 2 h to give a white precipitate. This solid crude product was centrifuged, washed with deionized water and ethanol, and dried in air to yield the as-prepared MSNs. To remove the surfactant template (CTAB), the as-prepared MSNs were calcined at 550 °C under oxygen for 5 h.

2.3. Synthesis of APTES-MSNs and PAH-cit/APTES-MSNs. Calcined MSNs (0.1 g) were refluxed for 24 h in anhydrous toluene (80.00 mL) and APTES (0.75 mL) to yield 3-aminopropyl-functionalized MSNs (APTES-MSNs). After centrifugation and washing, the purified APTES-MSNs were dried in air. To assemble the PAH-cit−APTES-MSNs shell−core structure, APTES-MSNs (20 mg) dissolved in 4-(2-hydroxyethyl)piperazine-1-ethanesulfonic acid (HEPES) buffer (3 mL, 10 mM, pH 7.4) were mixed with PAH-cit (10 mg) dispersed in a HEPES buffer (1 mL, 10 mM, pH 7.4) and stirred for 12 h. Finally, the synthesized PAH-cit/APTES-MSNs were freeze-dried.

2.4. Characterization. Transmission electron microscopy (TEM) images were obtained on a JEM 2011 transmission electron microscope (JEOL, Japan). Scanning electron microscopy (SEM) images were obtained on a XL 30 scanning electron microscope (Philips, Amsterdam, The Netherlands). Dynamic light scattering (DLS) and ζ-potential measurements were conducted on a Malvern Zetasizer (Nano series, Malvern Instruments Inc., Westborough, MA).

UV–vis absorption spectra were recorded on an Agilent 8453 UV–vis spectrophotometer. Fourier transform infrared (FT-IR) absorption spectra were recorded on a Nicolet Nexus 470 spectrometer. Thermogravimetric analysis (TGA) was conducted on a PerkinElmer TGA7; the samples were heated at a rate of 10 °C/min under air flow. Nitrogen sorption isotherms were measured at 77 K on a Micromeritics TriStar 3000 analyzer. The surface areas were calculated using the Brunauer–Emmett–Teller (BET) model, and the pore-size distributions were calculated using the Barrett–Joyner–Halenda (BJH) model.

2.5. DOX Loading and Release. PAH-cit/APTES-MSNs (10 mg) were added to DOX (12 mL, 5.0 mg) in a HEPES buffer (10 mM, pH 7.4). After the mixture was stirred for 24 h in the dark, the final mixture was centrifuged and washed with a HEPES buffer solution. The amount of DOX loaded into the MSNs was determined by subtracting the mass of DOX in the supernatant from the total mass of DOX determined by UV–vis spectroscopy at 480 nm. In the release experiments, two batches of DOX@PAH-cit/APTES-MSNs (10 mg) were suspended in a phosphate-buffered saline (PBS) solution (4 mL) at respective pH values of 7.4 and 5.5. The suspensions were transferred into a dialysis bag (M_w = 14000) and placed in a beaker containing 100 mL of buffer at the same pH condition. At fixed time intervals, 1 mL of solution was withdrawn from the beaker, and the same volume of fresh corresponding buffer was added to the original suspension. The amount of DOX was determined by UV–vis spectroscopy. For the measurements, standard curves were established at pH 7.4 and 5.5.

2.6. Cell Culture. HeLa cells were cultured at 37 °C in flasks containing DMEM and 10% FCS in a humidified atmosphere and 5% CO_2 in a Thermo culturist.

2.7. Cytotoxicity Assay. Cytotoxicity was determined by an MTT assay. HeLa cells were first seeded at 10^4 per cell in a 96-well cell culture plate in DMEM and 10% FCS at 37 °C and 5% CO_2 for 24 h. Then, different concentrations of materials were added after incubation for 24 h. MTT (100 μL, 5 mg/mL) was added and incubated for 4 h. Finally, the formed formazan was dissolved in dimethyl sulfoxide. The absorbance at 492 nm was recorded on an automatic ELISA analyzer (SPR-960).

2.8. CLSM of Subcellular Localization of DOX@PAH-cit/APTES-MSNs. HeLa cells were grown in DMEM supplemented with 10% FCS at 37 °C and 5% CO_2. Cells were seeded on 15 mm glass-bottom Petri dishes and allowed to adhere for 24 h. After 24 h of incubation, the cells were washed with a PBS solution three times. Then, HeLa cells were incubated with DOX@PAH-cit/APTES-MSNs in DMEM–10% FCS for a fixed time at 37 °C under 5% CO_2. After incubation, the cells were fixed with 4% paraformaldehyde in PBS for 15 min at 37 °C and stained with DAPI (0.2 μg/mL) in PBS for 20 min at 37 °C. Confocal fluorescence imaging was performed on a Leica laser scanning confocal microscope (Leica TCS SP5) using a 40× objective lens. The excitation of DAPI was 405 nm, and the fluorescence emission was monitored in the range of 430−450 nm. The excitation of DOX was 488 nm, and the fluorescence emission was monitored in the range of 550−700 nm.

2.9. In Situ Monitoring of Intracellular DOX Release Using CLSM. The in situ release monitoring study was performed using a confocal microscope; the temperature was set at 37 °C, and the concentration of CO_2 was 5% (in volume). The observation period was 24 h, and the fluorescence images were collected automatically every 30 min. The excitation of DAPI was 405 nm, and the fluorescence emission was monitored in the range of 430−450 nm. The excitation of DOX was 488 nm, and the fluorescence emission was monitored in the range of 550−700 nm.

3. RESULTS AND DISCUSSION

3.1. Synthesis and Characterization of PAH-cit/APTES-MSNs. The fabrication process of the DOX@PAH-cit/APTES-MSNs nanocomposite is shown in Figure 1b. MSNs were synthesized using a base-catalyzed sol–gel process.[48] The SEM image in Figure 2a shows that the MSNs are uniform in size
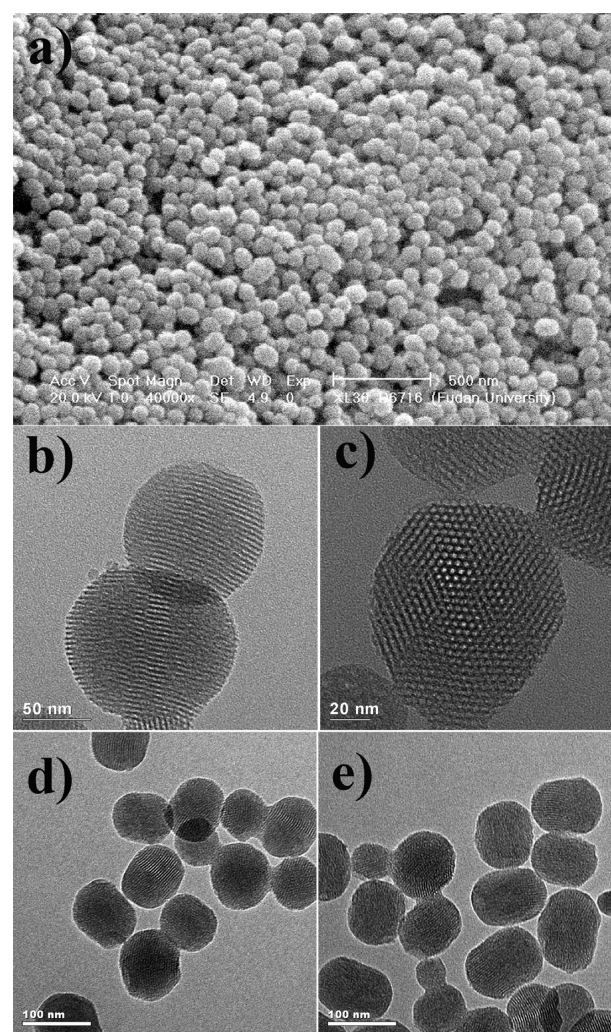

Figure 2. (a) SEM image of as-prepared MSNs (scale bar: 500 nm). TEM images showing (b) aligned stripelike features in as-prepared MSNs (scale bar: 50 nm) and (c) hexagonally packed light dot features in as-prepared MSNs (scale bar: 20 nm). TEM images of (d) APTES-modified MSNs (scale bar: 100 nm) and (e) PAH-cit/APTES-MSNs (scale bar: 100 nm).

(~100 nm). The ordered, two-dimensional hexagonal meso-porous structure was confirmed by TEM (Figure 2b,c). The nitrogen adsorption−desorption isotherm (Figure S1 in the Supporting Information, SI) further indicated that the synthesized silica NPs possessed mesoporous structures. The BET surface area, BJH pore volume, and pore diameter of the MSNs were 1320 m^2/g, 1.029 cm^3/g, and 2.2 nm, respectively.

Following calcination, MSNs were modified with APTES to obtain amino-functionalized MSNs (APTES-MSNs). Then, PAH-cit was added and adsorbed onto the outer and inner surfaces of APTES-MSNs through electrostatic forces. TEM images showed there were no differences in the MSNs morphology following modification with APTES and PAH-cit (Figure 2d,e); in order to get to know the thickness of the APTES and PAH-cit shells, high-resolution TEM (HRTEM) was applied, but it was still hard to "see" those shells (Figure S2 in the SI). These results suggest that the functionalized APTES and PAH-cit layers are extremely thin.

The FT-IR spectra of as-prepared MSNs, calcined MSNs, APTES-MSNs, and PAH-cit/APTES-MSNs are shown in Figure 3a. As-prepared MSNs displayed strong absorption
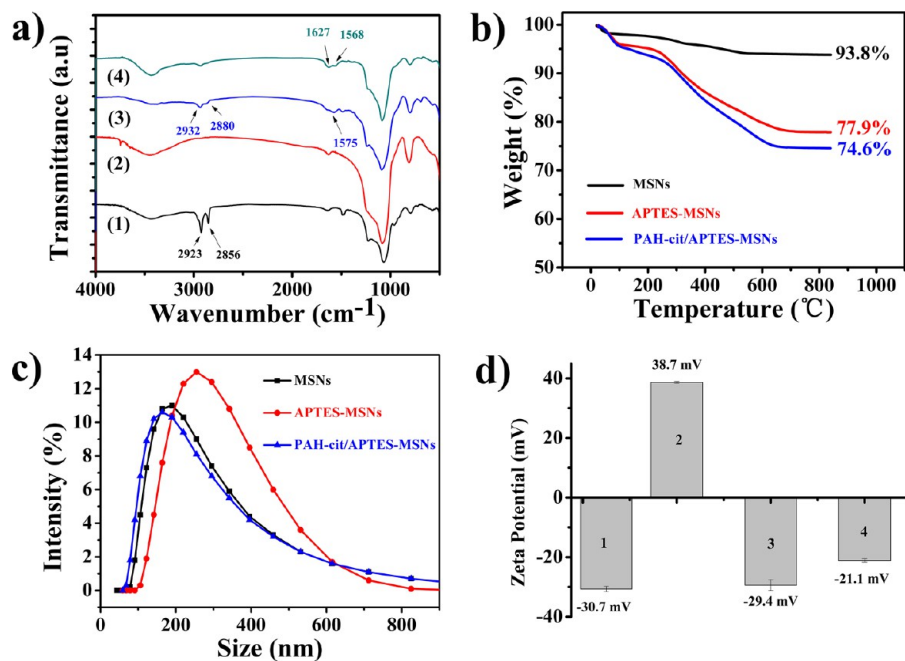
Figure 3. (a) FT-IR spectra of as-prepared MSNs (curve 1), calcined MSNs (curve 2), APTES-MSNs (curve 3), and PAH-cit/APTES-MSNs (curve 4). (b) TGA curves of calcined MSNs, APTES-MSNs, and PAH-cit/APTES-MSNs. (c) DLS profiles of calcined MSNs, APTES-MSNs, and PAH-cit/APTES-MSNs. (d) ζ-potential measurements of calcined MSNs (1), APTES-MSNs (2), PAH-cit/APTES-MSNs (3), and DOX@PAH-cit/APTES-MSNs (4) in a 10 mM HEPES buffer at pH 7.4.
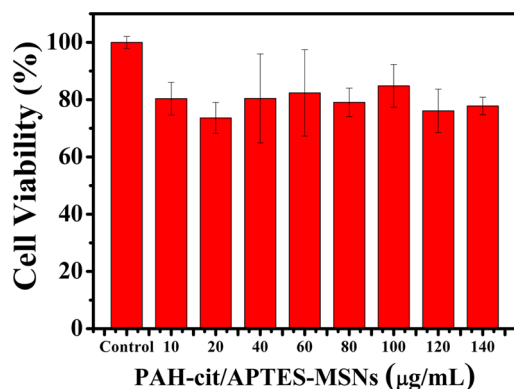

Figure 4. Cytotoxicity assay of HeLa cells treated with PAH-cit/APTES-MSNs.

signals at 2923 and 2856 cm^{-1}, which were assigned to the characteristic C−H stretching vibration of CTAB. Following calcination, those peaks disappeared, and the broad absorption band in the range of 3000−4000 cm^{-1} was assigned to the stretching vibration of the silanol group. Compared with calcined MSNs, APTES-MSNs displayed an additional peak at 1575 cm^{-1}, which was assigned to the N−H asymmetric bending vibration, and two peaks at 2932 and 2880 cm^{-1}, which were assigned to C−H stretching vibrations. Following modification with PAH-cit, absorption peaks at 1568 and 1627 cm^{-1} were observed and respectively assigned to the N−H bending and C=O stretching vibrations of PAH-cit (Figure S3 in the SI).

The adsorbed amount of PAH-cit onto MSNs was estimated by TGA. Following heating to 800 °C, MSNs, APTES-MSNs, and PAH-cit/APTES-MSNs displayed total weight losses of 6.2, 22.1, and 25.4 wt %, respectively (Figure 3b). Hence, the amount of adsorbed PAH-cit was 3.3 wt %.
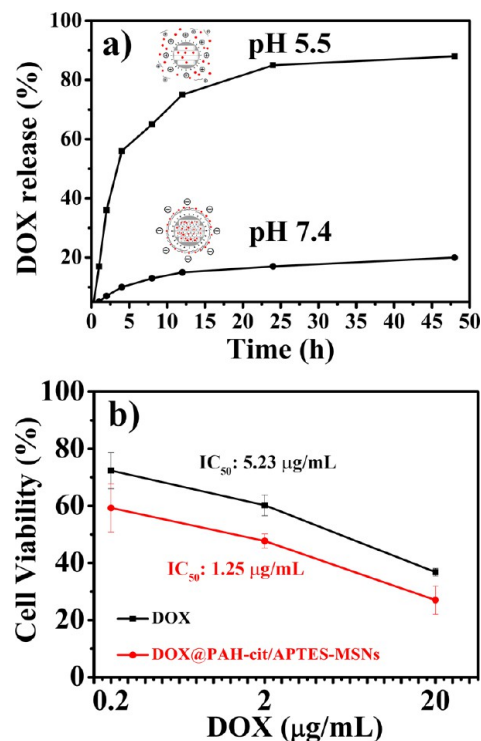

Figure 5. (a) DOX release profiles of the DOX@PAH-cit/APTES-MSNs nanocomposite at pH 5.5 and 7.4. (b) Cytotoxicity assay of HeLa cells treated with DOX@PAH-cit/APTES-MSNs and pure DOX.

As shown in Figure 3c, the diameters of MSNs and APTES-MSNs were 222.7 and 302.6 nm, as measured by DLS, and were larger than those observed from TEM analysis. This discrepancy can be ascribed to the following reasons: (1) the existence of a hydrate layer in aqueous solution; (2) the
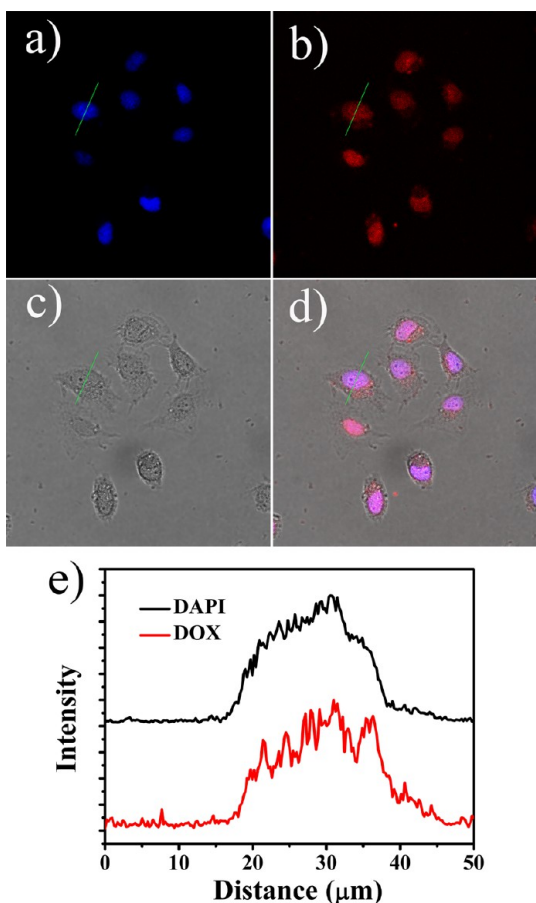
Figure 6. Confocal fluorescence images of living HeLa cells incubated with the DOX@PAH-cit/APTES-MSNs nanocomposite at 37 °C: (a) cell nucleus; (b) DOX; (c) bright-field images; (d) merged images; (e) luminescence intensity profiles obtained along the lines shown in the confocal fluorescence images.

reduced dispersibility of MSNs during the calcination and amination processes. In contrast, the PAH-cit/APTES-MSNs were smaller (203.6 nm in DLS diameter), indicating that PAH-cit/APTES-MSNs possessed better dispersibility in water compared with MSNs and APTES-MSNs due to the hydrophilic PAH-cit chains. ζ-potential tests were conducted, and the results are shown in Figure 3d. Because of the presence of silanol groups ($pK_a = 7.0$) on MSNs, the ζ potential of MSNs was about −30.7 mV. Following amination with APTES ($pK_a = 9.0$), the ζ potential of APTES-MSNs increased to 38.7 mV,

indicating successful modification with APTES on the internal and external surfaces of MSNs. Upon adsorption of PAH-cit, the ζ potential decreased to −29.4 mV. Thus, the results discussed above confirmed the successful fabrication of polymer-coated MSNs.

3.2. In Vitro PAH-cit/APTES-MSNs Cytotoxicity and DOX Loading/Release Evaluation. The cytotoxicity of PAH-cit/APTES-MSNs was investigated to examine their biocompatibility. Cell proliferation was assessed using HeLa cells and an MTT assay. The viability of untreated cells was assumed to be 100%. Following HeLa cell incubation with a series of PAH-cit/APTES-MSNs solutions at different concentrations, 10−140 μg/mL, for 24 h, no obvious cytotoxic effects were observed (Figure 4). This result clearly demonstrates that the synthesized PAH-cit/APTES-MSNs are biocompatible and suitable for use as DDSs.

To establish whether the DOX molecules were encapsulated in the MSNs channels or adsorbed onto the PAH-cit layer on the MSNs surfaces, ζ-potential and pore-volume measurements were obtained. Prior to DOX loading, the pore volume of PAH-cit/APTES-MSNs was 0.434 cm^3/g. Following DOX loading, the pore volume of DOX@PAH-cit/APTES-MSNs was 0.037 cm^3/g. This result demonstrated that DOX was successfully loaded into the pores. The ζ potentials before and after DOX loading were −29.4 and −21.1 mV, respectively (Figure 3d), indicating that some of the DOX molecules were additionally adsorbed on the MSN surface. The drug loading content, which accounts for DOX loaded into the pores and adsorbed onto the surface of PAH-cit/APTES-MSNs, was about 17.9 wt % using the established standard curves of DOX in different buffer solutions (Figure S4 in the SI). Fluorescence emission spectra were recorded for both free DOX and DOX@PAH-cit/APTES-MSNs and are shown in Figure S5 in the SI. Although the concentration of DOX (25 μg/mL) was the same in both samples, the fluorescence emission intensities were different. The free DOX sample exhibited considerably higher fluorescence intensities relative to the DOX-loaded PAH-cit/APTES-MSNs sample. This phenomenon can be explained by the fact that the DOX molecules were in close proximity both in the pores and on the surface of MSNs, which resulted in energy transfer between them, consequently causing self-quenching and reduced fluorescence emission intensity.

To investigate the drug-release behavior, DOX@PAH-cit/APTES-MSNs were dispersed in PBS buffer solutions at different pHs (5.5 and 7.4) and room temperature. As observed in Figure 5a, the drug-release rate of DOX@PAH-cit/APTES-MSNs was pH-dependent and increased at lower pHs. After
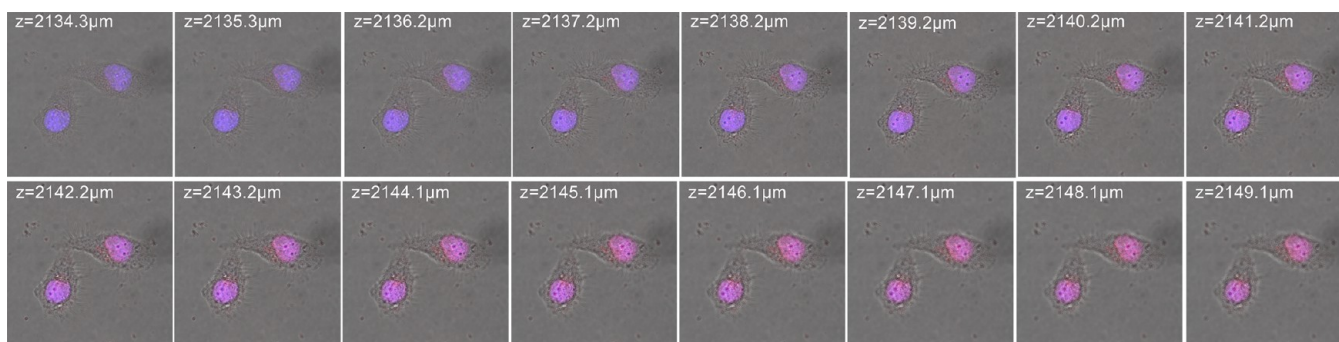

Figure 7. *Z*-axis confocal images of DOX@PAH-cit/APTES-MSNs nanocomposite uptake by HeLa cells. Purple emission is due to the combined blue (DAPI) and red (DOX) emissions.
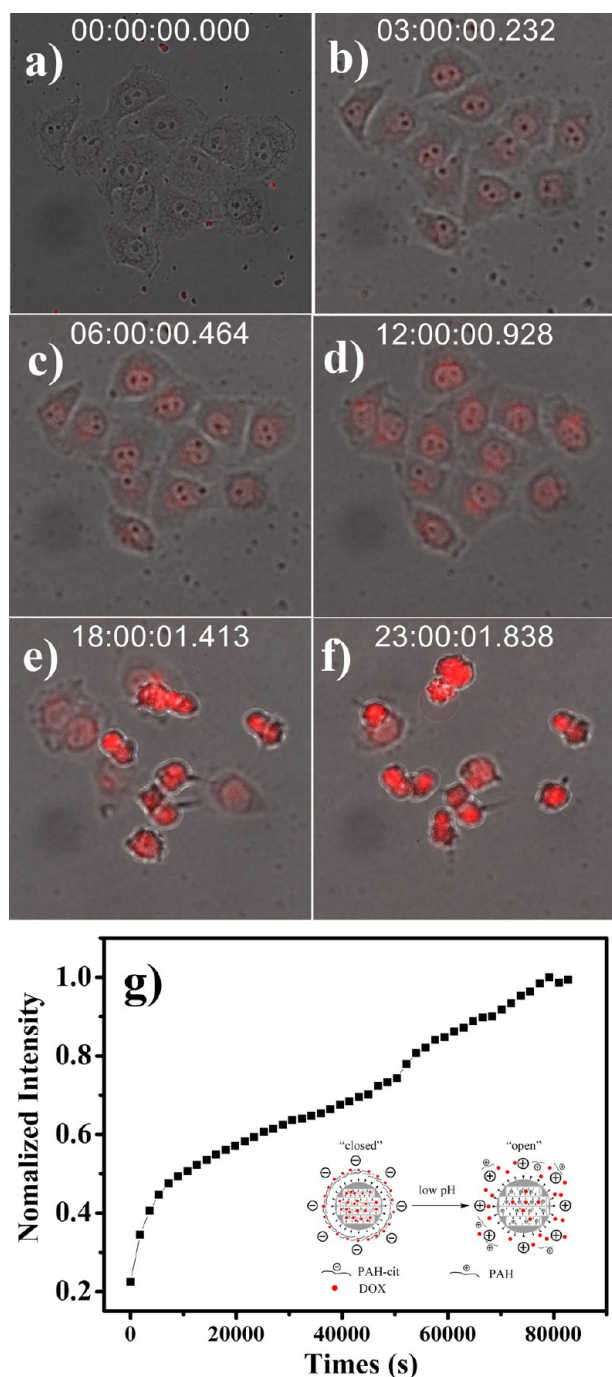
Figure 8. In situ monitoring of DOX@PAH-cit/APTES-MSNs nanocomposite uptake by HeLa cells and DOX release to the cell nucleus using CLSM: (a−f) confocal images of DOX@PAH-cit/APTES-MSNs nanocomposite uptake by HeLa cells at 0, 3, 6, 12, 18, and 23 h; (g) real-time monitoring of the intracellular DOX fluorescence intensity.

PAH-cit (negative) transformed to PAH (positive) under an acidic solution, there were two main forces that pushed the cationic DOX away from the MSNs: electrostatic repulsive forces (generated by positively charged APTES-MSNs and cationic DOX) and the driving force (due to the DOX's concentration differences inside and outside the MSNs), respectively. On the contrary, small anions such as the chloride anions will enter into the positively charged aminated MSNs (APTES-MSNs) when the positive PAH and DOX were

released out of the APTES-MSNs. After 48 h, the amount of DOX released reached 88% at pH 5.5. In contrast, only less than 20% of DOX was released at pH 7.4. This in vitro experiment demonstrated that at lower pHs the anionic PAH-cit gradually converted into cationic PAH and the loaded DOX could be released from the pores of MSNs under the influence of electrostatic repulsive forces. Lu et al.[49] synthesized pH-sensitive, polymer-conjugated hollow MSNs for controlled DOX release. The in vitro DOX release test showed that ~50% of the loaded drug was released within 24 h in a weak acidic environment (pH 5.6). Shi et al.[50] also fabricated pH-dependent DDSs using PEGylated MSNs as carriers. The data showed that when the pH was lowered to 5.4, only 15% of DOX was released at the 24-h mark. Compared with the literature DDSs mentioned above, the current DOX@PAH-cit/APTES-MSNs show more potential in drug-release applications under the same acidic conditions, suggesting that the loaded drug can be released to the outer environment more easily upon rupture of the polymer shell from the MSNs.

Figure 5b shows the in vitro cytotoxicity of pure DOX and DOX@PAH-cit/APTES-MSNs at different DOX concentrations. The cytotoxicity of DOX and DOX@PAH-cit/APTES-MSNs increased with increasing DOX concentrations. Significant growth inhibition of the HeLa cells was observed when their concentration reached 20 μg/mL (concentration of the drug). Only 27% of the cells remained viable following treatment with DOX@PAH-cit/APTES-MSNs for 24 h. In contrast, the cell viability was ~36.8% when the cells were treated with pure DOX.

3.3. Intracellular Monitoring of DOX@PAH-cit/APTES-MSNs. The cellular uptake and intracellular transport of DOX@PAH-cit/APTES-MSNs are important for efficient drug delivery. First, we investigated the transport ability of the DOX@PAH-cit/APTES-MSNs nanocomposite. As shown in Figure 6, the cell nucleus was stained with DAPI and showed blue luminescence. Following incubation with DOX@PAH-cit/APTES-MSNs, red luminescence originating from DOX was additionally observed in the nucleus of the HeLa cells and overlapped with blue luminescence, resulting in purple emission. The result indicated that, following transport to the cytoplasm, DOX was released from DOX@PAH-cit/APTES-MSNs and gradually diffused into the nucleus.

To determine the source of DOX activity, following DOX release, the intracellular location of DOX in a single cell was investigated by CLSM using line-scan fluorescent microscopy, which gave information about the spatial distribution of DOX inside the HeLa cells. As observed in Figure 6e, quantification of the luminescence intensity profile of DOX@PAH-cit/APTES-MSNs-treated HeLa cells revealed that most of the released DOX molecules were located in the cell nucleus. Z-axis fluorescence microscopy (Figure 7 and video S1 and single-channel images in Figure S6 in the SI) further confirmed the location of the released DOX molecules. DOX, an anticancer drug, is known to interfere with the double-stranded DNA in the nucleus, thus inhibiting the activities of topoisomerase.[51] Therefore, it can be deduced that the cell nucleus is the source of activity of DOX following its release.

3.4. In Situ Monitoring of DOX Release to the Nucleus of HeLa Cells. Because of the different fluorescent intensities between the loaded and released DOX, as shown in Figure S4 in the SI, the entire release process can be monitored under CLSM. As shown in Figure 8a−f, initially, nearly no luminescence was detected inside the cells. Subsequent

incubation for 3 h resulted in a weak red luminescence inside the cell nucleus, indicating that DOX was released from the endocytozed nanocomposite and diffused into the cell nucleus. Under prolonged incubation, the luminescence intensified and became brighter. At the 23-h mark, almost all of the cells were dead (video S2 in the SI). Figure 8g further indicated that, under extended incubation, DOX was gradually delivered and released to the cell nucleus. Furthermore, at the 23-h mark, the DOX fluorescence intensity inside the cells reached a plateau.

4. CONCLUSIONS

We have successfully developed a nanocomposite-based DDS. This is the first example of a pH-responsive charge-reversal polymer combined with MSNs reported for use in drug delivery. MTT results demonstrated that the nanocomposite has good biocompatibility; following DOX loading, the latter could effectively kill malignant cells. In comparison with previously reported nanocomposite-based DDSs, the present system has three advantages. First, the nanocomposite fabrication is relatively easy. Relative to tedious pH-sensitive linker syntheses, the current electrostatic adsorption approach is time-saving and simpler. Second, the released cationic polymer disrupts the endosomes and promotes the release of drug and subsequent diffusion to the nucleus. Third, owing to the different fluorescence intensities between the loaded and released DOX, the intracellular drug release process can be visualized by CLSM in real time.

■ ASSOCIATED CONTENT

Ⓢ Supporting Information

BET nitrogen adsorption−desorption isotherm and BJH pore-size distribution of calcined MSNs, HRTEM images of APTES-MSNs and PAH-cit/APTES-MSNs, FT-IR spectrum of PAH-cit, standard curves of UV−vis for DOX under pH 5.5 and 7.4, DOX fluorescence emission intensities before and after loading into PAH-cit/APTES-MSNs, single channels of Z-axis confocal images of DOX@PAH-cit/APTES-MSNs nanocomposite uptake by HeLa cells, video of Z-axis confocal microscopy, and video of real-time confocal microscopy. This material is available free of charge via the Internet at http://pubs.acs.org.

■ AUTHOR INFORMATION

Corresponding Author

* E-mail: jlkong@fudan.edu.cn. Tel.: +86-021-65642138. Fax: +86-021-65641740.

Notes

The authors declare no competing financial interest.

■ ACKNOWLEDGMENTS

■ REFERENCES

(1) Matsumura, Y.; Maeda, H. A New Concept for Macromolecular Therapeutics in Cancer Chemotherapy: Mechanism of Tumoritropic Accumulation of Proteins and the Antitumor Agent Smancs. *Cancer Res.* **1986**, *46*, 6387−6392.

(2) Hosta-Rigau, L.; Chandrawati, R.; Saveriades, E.; Odermatt, P. D.; Postma, A.; Ercole, F.; Breheney, K.; Wark, K. L.; Stadler, B.; Caruso, F. Noncovalent Liposome Linkage and Miniaturization of Capsosomes for Drug Delivery. *Biomacromolecules* **2010**, *11*, 3548−3555.

(3) Zhu, S. J.; Hong, M. H.; Tang, G. T.; Qian, L. L.; Lin, J. Y.; Jiang, Y. Y.; Pei, Y. Y. Partly PEGylated Polyamidoamine Dendrimer for Tumor-Selective Targeting of Doxorubicin: The Effects of PEGylation Degree and Drug Conjugation Style. *Biomaterials* **2010**, *31*, 1360−1371.

(4) Wang, Y. C.; Liu, X. Q.; Sun, T. M.; Xiong, M. H.; Wang, J. Functionalized Micelles from Block Copolymer of Polyphosphoester and Poly(ε-caprolactone) for Receptor-Mediated Drug Delivery. *J. Controlled Release* **2008**, *128*, 32−40.

(5) Xiong, X. B.; Lavasanifar, A. Traceable Multifunctional Micellar Nanocarriers for Cancer-Targeted Co-Delivery of MDR-1 siRNA and Doxorubicin. *ACS Nano* **2011**, *5*, 5202−5213.

(6) Shen, Y. Q.; Zhuo, Z. X.; Sui, M. H.; Tang, J. B.; Xu, P. S.; Van Kirk, E. A.; Murdoch, W. J.; Fan, M. H.; Radosz, M. Charge-Reversal Polyamidoamine Dendrimer for Cascade Nuclear Drug Delivery. *Nanomedicine* **2010**, *5*, 1205−1217.

(7) Vallet-Regi, M.; Ramila, A.; del Real, R. P.; Perez-Pariente, J. A New Property of MCM-41: Drug Delivery System. *Chem. Mater.* **2001**, *13*, 308−311.

(8) Vallet-Regi, M. A.; Ruiz-Gonzalez, L.; Izquierdo-Barba, I.; Gonzalez-Calbet, J. M. Revisiting Silica Based Ordered Mesoporous Materials: Medical Applications. *J. Mater. Chem.* **2006**, *16*, 26−31.

(9) Slowing, I. I.; Trewyn, B. G.; Giri, S.; Lin, V. S. Y. Mesoporous Silica Nanoparticles for Drug Delivery and Biosensing Applications. *Adv. Funct. Mater.* **2007**, *17*, 1225−1236.

(10) Trewyn, B. G.; Giri, S.; Slowing, I. I.; Lin, V. S. Y. Mesoporous Silica Nanoparticle Based Controlled Release, Drug Delivery, and Biosensor Systems. *Chem. Commun.* **2007**, 3236−3245.

(11) Trewyn, B. G.; Slowing, I. I.; Giri, S.; Chen, H.-T.; Lin, V. S. Y. Synthesis and Functionalization of a Mesoporous Silica Nanoparticle Based on the Sol-Gel Process and Applications in Controlled Release. *Acc. Chem. Res.* **2007**, *40*, 846−853.

(12) Vallet-Regi, M.; Balas, F.; Arcos, D. Mesoporous Materials for Drug Delivery. *Angew. Chem., Int. Ed.* **2007**, *46*, 7548−7558.

(13) Slowing, I. I.; Vivero-Escoto, J. L.; Wu, C. W.; Lin, V. S. Y. Mesoporous Silica Nanoparticles as Controlled Release Drug Delivery and Gene Transfection Carriers. *Adv. Drug Delivery Rev.* **2008**, *60*, 1278−1288.

(14) Tu, H. L.; Lin, Y. S.; Lin, H. Y.; Hung, Y.; Lo, L. W.; Chen, Y. F.; Mou, C. Y. In Vitro Studies of Functionalized Mesoporous Silica Nanoparticles for Photodynamic Therapy. *Adv. Mater.* **2009**, *21*, 172−177.

(15) Lu, J.; Liong, M.; Li, Z. X.; Zink, J. I.; Tamanoi, F. Biocompatibility, Biodistribution, and Drug-Delivery Efficiency of Mesoporous Silica Nanoparticles for Cancer Therapy in Animals. *Small* **2010**, *6*, 1794−1805.

(16) Ashley, C. E.; Carnes, E. C.; Phillips, G. K.; Padilla, D.; Durfee, P. N.; Brown, P. A.; Hanna, T. N.; Liu, J. W.; Phillips, B.; Carter, M. B.; Carroll, N. J.; Jiang, X. M.; Dunphy, D. R.; Willman, C. L.; Petsev, D. N.; Evans, D. G.; Parikh, A. N.; Chackerian, B.; Wharton, W.; Peabody, D. S.; Brinker, C. J. The Targeted Delivery of Multicomponent Cargos to Cancer Cells by Nanoporous Particle-Supported Lipid Bilayers. *Nat. Mater.* **2011**, *10*, 389−397.

(17) Agostini, A.; Mondragon, L.; Bernardos, A.; Martinez-Manez, R.; Marcos, M. D.; Sancenon, F.; Soto, J.; Costero, A.; Manguan-Garcia, C.; Perona, R.; Moreno-Torres, M.; Aparicio-Sanchis, R.; Murguia, J. R. Targeted Cargo Delivery in Senescent Cells Using Capped Mesoporous Silica Nanoparticles. *Angew. Chem., Int. Ed.* **2012**, *51*, 10556−10560.

(18) Chen, M. J.; Huang, C. S.; He, C. S.; Zhu, W. P.; Xu, Y. F.; Lu, Y. F.; Glucose-Responsive, A. Controlled Release System Using Glucose Oxidase-Gated Mesoporous Silica Nanocontainers. *Chem. Commun.* **2012**, *48*, 9522−9524.

(19) Climent, E.; Martinez-Manez, R.; Sancenon, F.; Marcos, M. D.; Soto, J.; Maquieira, A.; Amoros, P. Controlled Delivery Using Oligonucleotide-Capped Mesoporous Silica Nanoparticles. *Angew. Chem., Int. Ed.* **2010**, *49*, 7281−7283.

17452

dx.doi.org/10.1021/am5059519 | *ACS Appl. Mater. Interfaces* 2014, 6, 17446−17453

(20) Mal, N. K.; Fujiwara, M.; Tanaka, Y. Photocontrolled Reversible Release of Guest Molecules from Coumarin-Modified Mesoporous Silica. *Nature* **2003**, *421*, 350−353.

(21) Popat, A.; Ross, B. P.; Liu, J.; Jambhrunkar, S.; Kleitz, F.; Qiao, S. Z. Enzyme-Responsive Controlled Release of Covalently Bound Prodrug from Functional Mesoporous Silica Nanospheres. *Angew. Chem., Int. Ed.* **2012**, *51*, 12486−12489.

(22) Ferris, D. P.; Zhao, Y. L.; Khashab, N. M.; Khatib, H. A.; Stoddart, J. F.; Zink, J. I. Light-Operated Mechanized Nanoparticles. *J. Am. Chem. Soc.* **2009**, *131*, 1686−1688.

(23) He, X. X.; Zhao, Y. X.; He, D. G.; Wang, K. M.; Xu, F. Z.; Tang, J. L. ATP-Responsive Controlled Release System Using Aptamer-Functionalized Mesoporous Silica Nanoparticles. *Langmuir* **2012**, *28*, 12909−12915.

(24) Vivero-Escoto, J. L.; Slowing, I. I.; Wu, C. W.; Lin, V. S. Y. Photoinduced Intracellular Controlled Release Drug Delivery in Human Cells by Gold-Capped Mesoporous Silica Nanosphere. *J. Am. Chem. Soc.* **2009**, *131*, 3462−3463.

(25) Yuan, Q.; Zhang, Y. F.; Chen, T.; Lu, D. Q.; Zhao, Z. L.; Zhang, X. B.; Li, Z. X.; Yan, C. H.; Tan, W. H. Photon-Manipulated Drug Release from a Mesoporous Nanocontainer Controlled by Azobenzene-Modified Nucleic Acid. *ACS Nano* **2012**, *6*, 6337−6344.

(26) Angelos, S.; Yang, Y. W.; Patel, K.; Stoddart, J. F.; Zink, J. I. pH-Responsive Supramolecular Nanovalves Based on Cucurbit[6]uril Pseudorotaxanes. *Angew. Chem., Int. Ed.* **2008**, *47*, 2222−2226.

(27) Aznar, E.; Marcos, M. D.; Martinez-Manez, R.; Sancenon, F.; Soto, J.; Amoros, P.; Guillem, C. pH- and Photo-Switched Release of Guest Molecules from Mesoporous Silica Supports. *J. Am. Chem. Soc.* **2009**, *131*, 6833−6843.

(28) Bhattacharyya, S.; Wang, H. S.; Ducheyne, P. Polymer-Coated Mesoporous Silica Nanoparticles for the Controlled Release of Macromolecules. *Acta Biomater.* **2012**, *8*, 3429−3435.

(29) Casasus, R.; Climent, E.; Marcos, M. D.; Martinez-Manez, R.; Sancenon, F.; Soto, J.; Amoros, P.; Cano, J.; Ruiz, E. Dual Aperture Control on pH- and Anion-Driven Supramolecular Nanoscopic Hybrid Gate-Like Ensembles. *J. Am. Chem. Soc.* **2008**, *130*, 1903−1917.

(30) Nguyen, T. D.; Leung, K. C. F.; Liong, M.; Pentecost, C. D.; Stoddart, J. F.; Zink, J. I. Construction of a pH-Driven Supramolecular Nanovalve. *Org. Lett.* **2006**, *8*, 3363−3366.

(31) Park, C.; Oh, K.; Lee, S. C.; Kim, C. Controlled Release of Guest Molecules from Mesoporous Silica Particles Based on a pH-Responsive Polypseudorotaxane Motif. *Angew. Chem., Int. Ed.* **2007**, *46*, 1455−1457.

(32) Giri, S.; Trewyn, B. G.; Stellmaker, M. P.; Lin, V. S. Y. Stimuli-Responsive Controlled-Release Delivery System Based on Mesoporous Silica Nanorods Capped with Magnetic Nanoparticles. *Angew. Chem., Int. Ed.* **2005**, *44*, 5038−5044.

(33) Hernandez, R.; Tseng, H. R.; Wong, J. W.; Stoddart, J. F.; Zink, J. I. An Operational Supramolecular Nanovalve. *J. Am. Chem. Soc.* **2004**, *126*, 3370−3371.

(34) Kim, H.; Kim, S.; Park, C.; Lee, H.; Park, H. J.; Kim, C. Glutathione-Induced Intracellular Release of Guests from Mesoporous Silica Nanocontainers with Cyclodextrin Gatekeepers. *Adv. Mater.* **2010**, *22*, 4280−4283.

(35) Lai, C. Y.; Trewyn, B. G.; Jeftinija, D. M.; Jeftinija, K.; Xu, S.; Jeftinija, S.; Lin, V. S. Y. A Mesoporous Silica Nanosphere-Based Carrier System with Chemically Removable Cds Nanoparticle Caps for Stimuli-Responsive Controlled Release of Neurotransmitters and Drug Molecules. *J. Am. Chem. Soc.* **2003**, *125*, 4451−4459.

(36) Liu, R.; Zhao, X.; Wu, T.; Feng, P. Y. Tunable Redox-Responsive Hybrid Nanogated Ensembles. *J. Am. Chem. Soc.* **2008**, *130*, 14418−14419.

(37) Luo, Z.; Cai, K. Y.; Hu, Y.; Zhao, L.; Liu, P.; Duan, L.; Yang, W. H. Mesoporous Silica Nanoparticles End-Capped with Collagen: Redox-Responsive Nanoreservoirs for Targeted Drug Delivery. *Angew. Chem., Int. Ed.* **2011**, *50*, 640−643.

(38) Nguyen, T. D.; Liu, Y.; Saha, S.; Leung, K. C. F.; Stoddart, J. F.; Zink, J. I. Design and Optimization of Molecular Nanovalves Based on Redox-Switchable Bistable Rotaxanes. *J. Am. Chem. Soc.* **2007**, *129*, 626−634.

(39) Nguyen, T. D.; Tseng, H. R.; Celestre, P. C.; Flood, A. H.; Liu, Y.; Stoddart, J. F.; Zink, J. I. A Reversible Molecular Valve. *Proc. Natl. Acad. Sci. U. S. A.* **2005**, *102*, 10029−10034.

(40) Schmaljohann, D. Thermo- and pH-Responsive Polymers in Drug Delivery. *Adv. Drug Delivery Rev.* **2006**, *58*, 1655−1670.

(41) Sun, J. T.; Hong, C. Y.; Pan, C. Y. Fabrication of PDEAEMA-Coated Mesoporous Silica Nanoparticles and pH-Responsive Controlled Release. *J. Phys. Chem. C* **2010**, *114*, 12481−12486.

(42) Tang, H. Y.; Guo, J.; Sun, Y.; Chang, B. S.; Ren, Q. G.; Yang, W. L. Facile Synthesis of pH Sensitive Polymer-Coated Mesoporous Silica Nanoparticles and Their Application in Drug Delivery. *Int. J. Pharm.* **2011**, *421*, 388−396.

(43) Yuan, L.; Tang, Q. Q.; Yang, D.; Zhang, J. Z.; Zhang, F. Y.; Hu, J. H. Preparation of pH-Responsive Mesoporous Silica Nanoparticles and Their Application in Controlled Drug Delivery. *J. Phys. Chem. C* **2011**, *115*, 9926−9932.

(44) Guo, S. T.; Huang, Y. Y.; Jiang, Q. A.; Sun, Y.; Deng, L. D.; Liang, Z. C.; Du, Q. A.; Xing, J. F.; Zhao, Y. L.; Wang, P. C.; Dong, A. J.; Liang, X. J. Enhanced Gene Delivery and siRNA Silencing by Gold Nanoparticles Coated with Charge-Reversal Polyelectrolyte. *ACS Nano* **2010**, *4*, 5505−5511.

(45) Han, L.; Zhao, J.; Zhang, X.; Cao, W. P.; Hu, X. X.; Zou, G. Z.; Duan, X. L.; Liang, X. J. Enhanced siRNA Delivery and Silencing Gold−Chitosan Nanosystem with Surface Charge-Reversal Polymer Assembly and Good Biocompatibility. *ACS Nano* **2012**, *6*, 7340−7351.

(46) Zhou, T.; Zhou, X.; Xing, D. Controlled Release of Doxorubicin from Graphene Oxide Based Charge-Reversal Nanocarrier. *Biomaterials* **2014**, *35*, 4185−4194.

(47) Liu, X. H.; Zhang, J. T.; Lynn, D. M. Polyelectrolyte Multilayers Fabricated from 'Charge-Shifting' Anionic Polymers: A New Approach to Controlled Film Disruption and the Release of Cationic Agents from Surfaces. *Soft Matter* **2008**, *4*, 1688−1695.

(48) Radu, D. R.; Lai, C. Y.; Jeftinija, K.; Rowe, E. W.; Jeftinija, S.; Lin, V. S. Y. A Polyamidoamine Dendrimer-Capped Mesoporous Silica Nanosphere-Based Gene Transfection Reagent. *J. Am. Chem. Soc.* **2004**, *126*, 13216−13217.

(49) Mei, X.; Chen, D. Y.; Li, N. J.; Xu, Q. F.; Ge, J. F.; Li, H.; Lu, J. M. Hollow Mesoporous Silica Nanoparticles Conjugated with pH-Sensitive Amphiphilic Diblock Polymer for Controlled Drug Release. *Microporous Mesoporous Mater.* **2012**, *152*, 16−24.

(50) Gu, J. L.; Su, S. S.; Zhu, M. J.; Li, Y. S.; Zhao, W. R.; Duan, Y. R.; Shi, J. L. Targeted Doxorubicin Delivery to Liver Cancer Cells by PEGylated Mesoporous Silica Nanoparticles with a pH-Dependent Release Profile. *Microporous Mesoporous Mater.* **2012**, *161*, 160−167.

(51) Han, S. Y.; Liu, Y. X.; Nie, X.; Xu, Q.; Jiao, F.; Li, W.; Zhao, Y. L.; Wu, Y.; Chen, C. Y. Efficient Delivery of Antitumor Drug to the Nuclei of Tumor Cells by Amphiphilic Biodegradable Poly(L-aspartic acid-*co*-lactic acid)/DPPE Co-Polymer Nanoparticles. *Small* **2012**, *8*, 1596−1606.